


# Cavin-2 promotes fibroblast-to-myofibroblast trans-differentiation and aggravates cardiac fibrosis

Yusuke Higuchi<sup>1</sup>, Takehiro Ogata<sup>1,2\*</sup> , Naohiko Nakanishi<sup>1</sup>, Masahiro Nishi<sup>1</sup>, Yumika Tsuji<sup>1</sup>, Shinya Tomita<sup>1</sup>, Simon J. Conway<sup>3</sup> and Satoaki Matoba<sup>1</sup>

<sup>1</sup>Department of Cardiovascular Medicine, Graduate School of Medical Science, Kyoto Prefectural University of Medicine, Kyoto, Japan; <sup>2</sup>Department of Pathology and Cell Regulation, Graduate School of Medical Science, Kyoto Prefectural University of Medicine, Kyoto, Japan; and <sup>3</sup>Herman B. Wells Center for Pediatric Research, Department of Pediatrics, Indiana University School of Medicine, Indianapolis, IN, USA

## Abstract

**Aims** Transforming growth factor  $\beta$  (TGF- $\beta$ ) signalling is one of the critical pathways in fibroblast activation, and several drugs targeting the TGF- $\beta$ /Smad signalling pathway in heart failure with cardiac fibrosis are being tested in clinical trials. Some caveolins and cavins, which are components of caveolae on the plasma membrane, are known for their association with the regulation of TGF- $\beta$  signalling. Cavin-2 is particularly abundant in fibroblasts; however, the detailed association between Cavin-2 and cardiac fibrosis is still unclear. We tried to clarify the involvement and role of Cavin-2 in fibroblasts and cardiac fibrosis.

**Methods and results** To clarify the role of Cavin-2 in cardiac fibrosis, we performed transverse aortic constriction (TAC) operations on four types of mice: wild-type (WT), Cavin-2 null (Cavin-2 KO), Cavin-2<sup>flox/flox</sup>, and activated fibroblast-specific Cavin-2 conditional knockout (Postn-Cre/Cavin-2<sup>flox/flox</sup>, Cavin-2 cKO) mice. We collected mouse embryonic fibroblasts (MEFs) from WT and Cavin-2 KO mice and investigated the effect of Cavin-2 in fibroblast trans-differentiation into myofibroblasts and associated TGF- $\beta$  signalling. Four weeks after TAC, cardiac fibrotic areas in both the Cavin-2 KO and the Cavin-2 cKO mice were significantly decreased compared with each control group (WT 8.04  $\pm$  1.58% vs. Cavin-2 KO 0.40  $\pm$  0.03%,  $P < 0.01$ ; Cavin-2<sup>flox/flox</sup>, 7.19  $\pm$  0.50% vs. Cavin-2 cKO 0.88  $\pm$  0.44%,  $P < 0.01$ ). Fibrosis-associated mRNA expression (*Col1a1*, *Ctgf*, and *Col3*) was significantly attenuated in the Cavin-2 KO mice after TAC.  $\alpha 1$  type I collagen deposition and non-vascular  $\alpha$ SMA-positive cells (WT 43.5  $\pm$  2.4% vs. Cavin-2 KO 25.4  $\pm$  3.2%,  $P < 0.01$ ) were reduced in the heart of the Cavin-2 cKO mice after TAC operation. The levels of  $\alpha$ SMA protein (0.36-fold,  $P < 0.05$ ) and fibrosis-associated mRNA expression (*Col1a1*, 0.69-fold,  $P < 0.01$ ; *Ctgf*, 0.27-fold,  $P < 0.01$ ; *Col3*, 0.60-fold,  $P < 0.01$ ) were decreased in the Cavin-2 KO MEFs compared with the WT MEFs. On the other hand,  $\alpha$ SMA protein levels were higher in the Cavin-2 overexpressed MEFs compared with the control MEFs (2.40-fold,  $P < 0.01$ ). TGF- $\beta$ 1-induced Smad2 phosphorylation was attenuated in the Cavin-2 KO MEFs compared with WT MEFs (0.60-fold,  $P < 0.01$ ). Heat shock protein 90 protein levels were significantly reduced in the Cavin-2 KO MEFs compared with the WT MEFs (0.69-fold,  $P < 0.01$ ).

**Conclusions** Cavin-2 loss suppressed fibroblast trans-differentiation into myofibroblasts through the TGF- $\beta$ /Smad signalling. The loss of Cavin-2 in cardiac fibroblasts suppresses cardiac fibrosis and may maintain cardiac function.

**Keywords** Cardiac fibrosis; Cavin-2; Fibroblasts; TGF- $\beta$ /Smad signalling

Received: 9 March 2023; Revised: 22 September 2023; Accepted: 8 October 2023

\*Correspondence to: Takehiro Ogata, Department of Pathology and Cell Regulation, Graduate School of Medical Science, Kyoto Prefectural University of Medicine, Kyoto 602-8566, Japan. Email: ogatat@koto.kpu-m.ac.jp

## Introduction

Cardiac fibrosis is an essential pathological process associated with impaired cardiac function and subsequent heart failure (HF),<sup>1</sup> which is one of the major causes of death worldwide.

Although several novel drugs, such as angiotensin receptor-neprilysin inhibitors and sodium/glucose cotransporter 2 inhibitors, improve the prognosis of patients with HF, about half of the patients with HF die within 5 years of diagnosis,<sup>2</sup> suggesting the insufficiency of modern therapy. The treatment

focused on cardiac fibrosis can improve the progression of patients with HF: However, despite intense research on cardiac fibrosis, effective anti-fibrosis treatments have not been established for clinical applications.<sup>3,4</sup> Therefore, understanding the detailed mechanisms of cardiac fibrosis and identifying novel modalities to regulate this process will have a substantial impact on the mechanism of HF and greatly help advance HF treatment.

Cardiac fibrosis is caused by fibroblast activation, and activated fibroblasts facilitate excessive extracellular matrix (ECM) accumulation and excessive ECM turnover.<sup>1</sup> Cardiac fibroblast activation strongly correlates with HF development,<sup>5,6</sup> and resident fibroblast plays pivotal roles for cardiac fibrosis in pressure over-loaded hearts.<sup>7,8</sup> The transforming growth factor  $\beta$  (TGF- $\beta$ ) family are central mediators of fibroblast activation, and TGF- $\beta$  signalling is implicated in myocardial infarction, pressure-overloaded hearts, and various cardiomyopathies.<sup>9</sup> However, long-term direct inhibition of TGF- $\beta$  signalling has a risk of unacceptable adverse effects.<sup>10</sup> TGF- $\beta$  signalling pathway is affected by heat shock protein 90 (HSP90) activity in renal fibrosis, dermal fibrosis, cancer cell lines, and idiopathic pulmonary fibrosis.<sup>11–14</sup> HSP90 inhibition attenuated fibroblast activation, myofibroblast accumulation, and collagen deposition without any detectable toxic effects in pulmonary fibrosis.<sup>15</sup> Accordingly, the anti-fibrosis therapies indirectly targeting the TGF- $\beta$  signalling pathway potentially apply to the treatment of HF.

Caveola is a cholesterol-rich membrane microdomain that acts as a signalling platform in facilitating specific signal transduction events. Coat proteins, caveolins, and adaptive proteins, cavins, modulate the morphology and functions of caveolae. Caveolin-1 interacts with the Type I TGF- $\beta$  receptor and suppresses the downstream signalling of the TGF- $\beta$  pathway.<sup>16</sup> Caveolin-1 also affects epithelial–mesenchymal transition and endothelial–mesenchymal transition.<sup>17,18</sup> Previously, we showed that Cavin-1 and Cavin-4 affect cardiomyocyte function and cardiac fibrosis.<sup>19,20</sup> Cavin-2 is expressed in various cells and is also expressed in human and mouse fibroblasts.<sup>21</sup> Because previous studies showed that Cavin-2 was crucial for proliferation, migration, and invasion in the endothelial cells<sup>22</sup> and adipocyte differentiation,<sup>23</sup> Cavin-2 may be directly involved in intra-fibroblast signalling essential for cardiac fibrosis, as well as endothelial cells and adipocytes. However, the role of Cavin-2 in cardiac fibroblasts remains unclear.

Here, we demonstrate a role for Cavin-2 in the trans-differentiation from fibroblast to myofibroblast. Cavin-2 deficiency attenuates TGF- $\beta$ /Smad signalling with the reduction of HSP90. In addition, activated-fibroblast-selective Cavin-2 knockout mice reveal attenuated cardiac fibrosis and preserved cardiac function in the pressure-overloaded HF. Our results indicate that Cavin-2 is essential in the early stages of fibrosis and a potential therapeutic target for treating fibrosis.

## Material and methods

### Reagents

The rabbit polyclonal antibodies to ERK (#9102), phospho-ERK (#9101), Akt (#9272), phospho-Akt (#9271), Smad2 (#5339), phospho-Smad2 (#3108), phospho-Smad2/3 (#9510), and the horseradish peroxidase-conjugated secondary antibodies [anti-mouse-HRP (#7076S), and anti-rabbit-HRP (#7074S)] were purchased from Cell Signalling Technology, Inc. (Danvers, MA, USA); the rabbit polyclonal antibody to Cavin-2 (12339-1-AP) was purchased from ProteinTech Group, Inc. (Rosemont, IL, USA); the rabbit polyclonal antibodies to  $\alpha$  smooth muscle actin ( $\alpha$ SMA) (ab5694), the mouse monoclonal antibody to HSP90 (ab13492), and the horseradish peroxidase-conjugated monoclonal antibody to GAPDH (ab9385) were from Abcam plc (Cambridge, UK); the Cy3-conjugated mouse monoclonal antibody to  $\alpha$ SMA (C6198) was purchased from Sigma-Aldrich Co. (St. Louis, MO, USA). TRIzol was obtained from Thermo Fisher Scientific Inc. (Waltham, MA, USA). Dulbecco's modified Eagle medium (DMEM), penicillin/streptomycin solution ( $\times 100$ ), phosphate-buffered saline, 4% paraformaldehyde, and isopropyl alcohol were purchased from FUJIFILM Wako Pure Chemical Corporation (Tokyo, Japan). DAPI Fluoromount-G<sup>®</sup> was purchased from Southern Biotech (Birmingham, AL, USA). Recombinant human TGF- $\beta$  protein was purchased from R&D Systems, Inc. (Minneapolis, MN, USA).

### Animals

Cavin-2 KO mice and Cavin-2<sup>fllox/fllox</sup> mice were generated as previously described.<sup>23</sup> Transgenic mice in which Cre recombinase is driven by a 3.9-kb mouse *Postn* promoter, named Postn-Cre mice, were generated by Dr. Conway and colleagues.<sup>24</sup> We generated mice with Cavin-2 loss in activated fibroblasts (Cavin-2 cKO) by breeding Cavin-2<sup>fllox/fllox</sup> mice with Postn-Cre mice. All aspects of animal care and experimentation performed in this study were approved by the Institutional Animal Care and Use Committee of Kyoto Prefectural University of Medicine. The investigation conforms to the Guide for the Care and Use of Laboratory Animals published by the US National Institutes of Health (NIH Publication No. 85-23, revised 1985).

### Transverse aortic constriction operation

Male C57BL/6 wild-type (WT), Cavin-2 KO, Cavin-2<sup>fllox/fllox</sup>, and Cavin-2 cKO mice at 8 to 10 weeks of age were subjected to transverse aortic constriction (TAC) or sham operation. In brief, mice were anaesthetized with 1.0% isoflurane and then given medetomidine (0.75 mg/kg) and butorphanol

(5.0 mg/kg) intraperitoneally for analgesia. Aortic constriction was performed by ligation of the transverse thoracic aorta between the innominate artery and left common carotid artery with a 27-gauge needle using a 6-0 silk string as previously described.<sup>25</sup> The pressure gradient in the thoracic aorta was measured by Doppler echocardiography to confirm significant pressure overload in both WT, Cavin-2 KO, Cavin-2<sup>flox/flox</sup>, and Cavin-2 cKO mice. The sham operation was identical, except that the thread was not ligated. Samples were obtained 4 weeks after the TAC or sham procedure.

### Mouse embryonic fibroblasts isolation

WT mouse embryonic fibroblasts (MEFs) and Cavin-2 KO MEFs were isolated from 13–14 days pregnant WT mice and Cavin-2 KO mice respectively as previously described.<sup>26</sup> MEFs were cultured from the embryo from which the head and the visible internal organs were removed. MEFs from WT and Cavin-2 KO mice were collected at the same time.

### Histological staining and analysis

Mouse heart samples were isolated, fixed with 4% paraformaldehyde at 4°C for 24 h, then embedded in paraffin, and sectioned at 5 µm. Masson's trichrome staining was performed to assess the degree of cardiac fibrosis. Picrosirius red staining was performed to identify collagen fibres, following the manufacturer's instructions. Picrosirius red-stained interstitial fibrosis was observed under light microscopy (BZ-X800, KEYENCE) at ×20 magnification. The percent area of extracellular Masson's trichrome staining was computed from 8 to 10 random fields within the mid-myocardium in each murine sample, in order to exclude large epicardial arteries/veins and any cutting/compression artefacts. Cardiac hypertrophy was evaluated in 100 to 200 cells from the cross-sectional area of cardiomyocytes for each mouse sample. The digital photomicrographs were quantified with Adobe Photoshop (Adobe Photoshop CC 2017).

### Immune-fluorescence staining

MEFs were fixed with 4% paraformaldehyde at room temperature for 15 min and stained with the anti-αSMA (1:200), anti-pSmad2/3 (1:200), or phalloidin (1:2000). Secondary antibodies were conjugated with Alexa Fluor 488 or 555 (1:500), and nuclei were visualized using DAPI Fluoromount-G®. Fluorescent signals were detected using a Zeiss LSM510 META Confocal Imaging System (Carl Zeiss, Jena, Germany) or a Keyence BZ-X700 digital microscope (Osaka, Japan).

### Transthoracic echocardiography

Mice were anaesthetized with 1.0% isoflurane inhalation. Echocardiographic analysis was performed with a Visual Sonics Vevo 2,100 equipped with an 18- to 38-MHz transducer (Visual Sonics, Toronto, ON, Canada). Left ventricular end-diastolic internal dimension, left ventricular systolic internal dimension, and diastolic left ventricular posterior wall were evaluated with M-mode tracing at the papillary muscle level of a parasternal short-axis view. Echocardiographic measurement was assessed 0, 2, and 4 weeks after the sham or TAC operation.

### Cell culture and induction of trans-differentiation

MEFs were maintained in DMEM containing 100 U/mL penicillin, and 100 mg/mL streptomycin, and supplemented with 10% (v/v) heat-inactivated fetal bovine serum at 37°C in a 5% CO<sub>2</sub> atmosphere. For investigating trans-differentiation, cells were induced 1-day post-confluence with DMEM supplemented with 10% FBS, 10 ng/mL TGF-β1, 100 U/mL penicillin, and 100 µg/mL streptomycin for 24 h.

### Gene transfer

Recombinant adenoviruses expressing HA-tagged human SDPR/Cavin-2 (Ad-Cavin-2-HA) and Ad-β-galactosidase (Ad-LacZ) were described previously.<sup>20</sup> Twenty-four hours after seeding on a plate, WT MEFs were infected with Ad-Cavin-2-HA or Ad-LacZ diluted in culture media at a multiplicity of infection of 30 and incubated at 37°C for 24 h. The viral suspension was removed, and the MEFs were cultured with fresh media.

### RNA isolation and gene expression analysis by qPCR or scRNA-seq

Reverse transcription-mediated quantitative polymerase chain reaction was conducted as described previously.<sup>20</sup> Total RNA was extracted from cultured cells or tissues using TRIzol and converted to cDNA using a high capacity cDNA reverse transcription kit (Applied Biosystems/Thermo Fisher Scientific, Foster City, CA, USA). Synthesized cDNA was analysed by kinetic real-time PCR using Takara PCR thermal cycler dice (Takara Bio Inc., Kusatsu, Japan) with Platinum SYBR Green qPCR Supermix (Invitrogen/Thermo Fisher Scientific). The primer sequences are provided in *Table S1*.

Heart tissue single-cell RNA-seq (scRNA-seq) data were accessed from the Tabula Muris data set (<https://tabula-muris.ds.czbiohub.org/>). These data were from the

mice hearts of four male and three female, chow-fed 10–15 weeks old C57BL/6JN mice obtained from Charles River Labs.<sup>27</sup>

## Western blot analysis

Cell lysates were extracted using a lysis buffer (50 mM Tris-HCl, pH 7.5, 150 mM NaCl, 50 mM EDTA, 1% Triton X-100 and protease-phosphatase inhibitor mixture). Protein samples were subjected to SDS-PAGE, then transferred to polyvinylidene difluoride membranes that were subsequently incubated with primary antibodies against phospho-Akt, Akt, phospho-ERK1/2, ERK1/2, phospho-Smad2, Smad2,  $\alpha$ SMA, HSP90, Cavin-2, and GAPDH. Horseradish peroxidase-conjugated anti-rabbit and anti-mouse IgG were used as secondary antibodies.

## Biotin identification screening

The Humanized BirA (hBirA) sequence was obtained from a previously published sequence<sup>28</sup> by adding a Kozac sequence at the 5' site and an EcoRI sequence at the 3' site. This sequence was inserted into pcDNA3.1(+)-HA (Clontech, CA, USA) to generate pcDNA3.1+/hBirA-HA. HA-tagged hBirA was cloned by PCR from the pcDNA3.1+/hBirA-HA plasmid with forward and reverse primers (F: 5'-TTAGATCTCTCGA-GGCCACCATGAAGGACAACACCGTGCC-3', R:5'-CCTACCCGG-TAGAATTCTCAAGCGTAATCTGGAACATCGTATGGGTACTTCT-GCGCTTCTCAGGG-3'). HA-tagged hBirA was inserted into pMSCV-puromycin to generate pMSCV-hBirA-HA-puromycin using the Gibson Assembly<sup>®</sup> kit (New England Biolabs, Ipswich, MA, USA). mCavin-2 was cloned by PCR from pEGFP-C1-mCavin-2 (Adgene 68398, Rob Parton) was inserted into pMSCV-hBirA-HA-puromycin to create pMSCV-hBirA-mCavin-2-HA-puromycin. MEFs expressing hBirA-HA or hBirA-mCavin-2-HA by retrovirus infection were incubated with 50  $\mu$ M biotin for 6 h. The lysate was collected and mixed with MagCapture Tamavidin2-REV beads (FUJIFILM Wako Pure Chemical Corporation, Tokyo, Japan) at 4°C overnight. The beads were washed with phosphate-buffered saline, and mass spectrometry was performed (CERI, Tokyo, Japan) as previously described. LC-MS/MS analyses were performed using a nano LC (UltiMate<sup>®</sup> 3,000). (Dionex, Sunnyvale, CA, USA) coupled with a Q Exactive Plus Orbitrap mass spectrometer (Thermo Scientific, Waltham, MA, USA). Instrument operation and data acquisition were performed using Xcalibur Software (Thermo Scientific, Waltham, MA, USA).

## LC-MS/MS data analysis

The MS/MS raw data were processed using Mascot version 2.6.0 (Matrix Sciences, London, US) and were searched in

the Swiss-Prot database with humans as the species, carbamidomethylation of cysteine as a static modification, oxidation of methionine as a dynamic modification, precursor mass tolerance of 1.0 Da, and a fragment mass tolerance of 0.8 Da. The dat files of all fractions obtained were processed with Scaffold version 5.0.1 (Proteome Software Inc.). The parameters of scaffold were adjusted as follows to ensure accurate identification of peptides and proteins: protein identifications were accepted if they were established with a probability greater than 99.9%, and peptide identifications were accepted if they contained at least four peptides identified with a probability >80% (using the Scaffold Local FDR algorithm). The normalized spectral abundance factor (Weighted Spectra) was calculated for each protein and compared between Cavin-2 and HA samples.

## Statistical analysis

The experiments were carried out at least three times unless otherwise stated. All data were expressed as mean  $\pm$  standard errors. Statistical analysis was performed by one-way ANOVA followed by Tukey's *post hoc* test, and *P*-values below 0.05 were considered significant. Statistical analyses were performed using GraphPad Prism 8 statistical packages (GraphPad Software, Inc.).

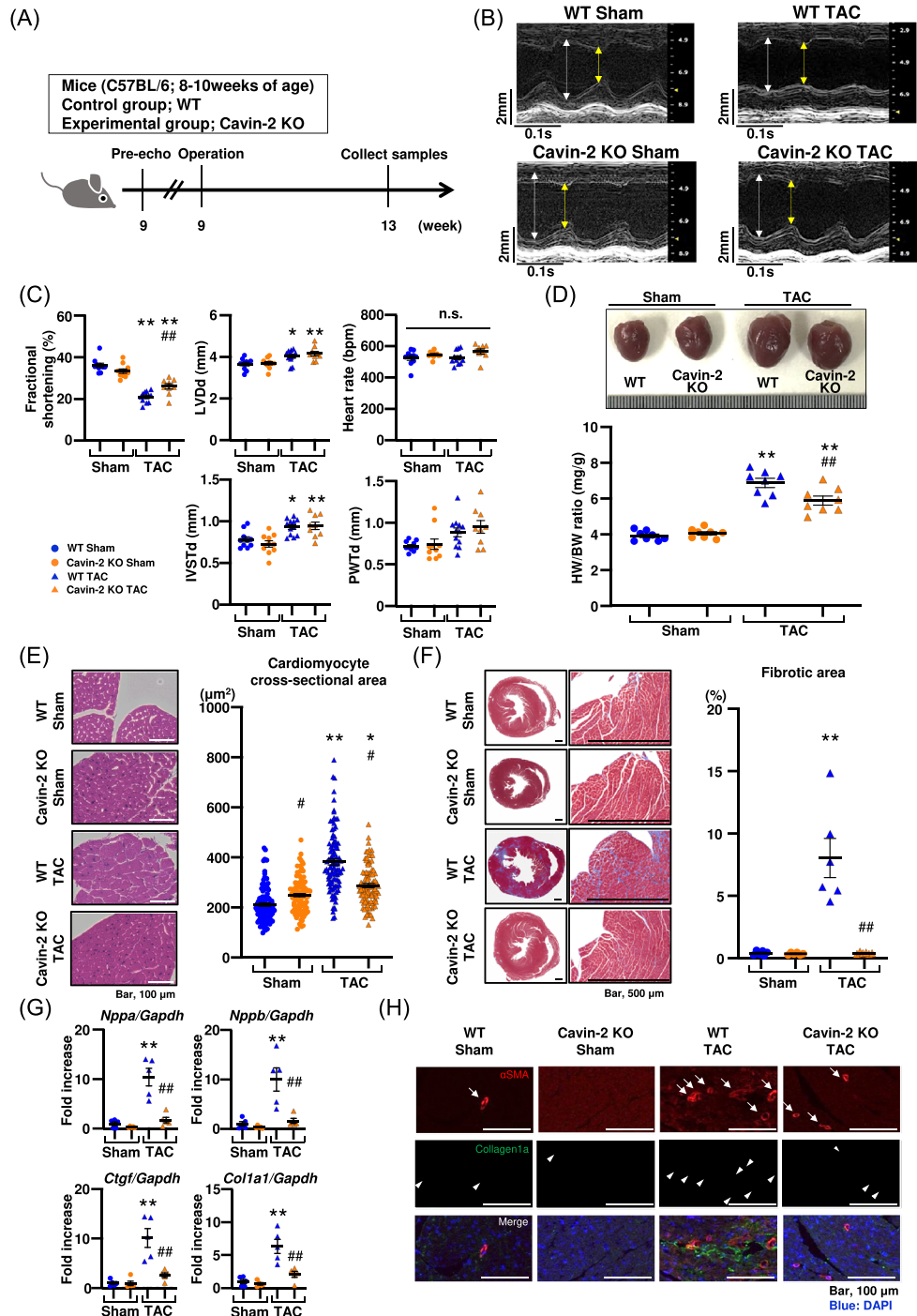
## Results

### Cavin-2 KO attenuates cardiac fibrosis in pressure-overload heart failure

We first used Cavin-2 KO mice to examine the involvement of Cavin-2 in the progression of HF and cardiac fibrosis. The cardiac function of the Cavin-2 KO mice was comparable with that of the WT mice (*Figure S1A*). We performed TAC operations to induce pressure-overload HF. Four weeks after the TAC operation, we confirmed the peak pressure gradient at the transverse aorta (*Figure S1B*) and evaluated their cardiac function (*Figure 1A*). A decrease in systolic function after TAC operation was observed in the WT mice, and it was attenuated in the Cavin-2 KO mice (*Figure 1B,C*). In the assessment of cardiac remodelling, cardiomyocyte hypertrophy and cardiac fibrosis following TAC operation were observed in the WT mice. They were attenuated in the Cavin-2 KO mice (*Figure 1D–F*). After TAC operation, the mRNA expression levels of cardiac remodelling and fibrosis-related genes (*Nppa*, *Nppb*, *Col1a1*, *Ctgf*, and *Col3*) were significantly suppressed in the Cavin-2 KO mice compared with the WT mice (*Figure 1G* and *Figure S1C*). Consistent with the attenuation of cardiac fibrosis by Cavin-2 loss, the number of  $\alpha$ SMA-positive myofibroblasts and collagen $\alpha$ 1



**Figure 1** Systemic Cavin-2 KO attenuates fibrosis and preserves function in the pressure-overloaded heart. Schematic of the experimental design (A) and representative M-mode images (B) and data (C) of echocardiography in wild-type (WT) and Cavin-2 KO mice 4 weeks after Sham or TAC operation (WT sham,  $n = 10$ ; Cavin-2 KO Sham,  $n = 10$ ; WT TAC,  $n = 12$ ; Cavin-2 KO TAC,  $n = 9$ ). (D) Gross appearance of whole heart (upper raw) and heart weight/body weight ratio (lower graph) of the mice ( $n = 8$  per group). Representative HE-stained sections of the heart and quantification of cardiomyocyte cross-sectional area (E) after 4 weeks of Sham or TAC operation, and Masson's trichrome staining and quantification of fibrotic area (F,  $n = 5$  per group). The scale bar is 100 or 500  $\mu\text{m}$ . (G) Relative mRNA expression of genes associated with heart failure (*Nppa* and *Nppb*) and fibrosis (*Ctgf* and *Col1a1*) in the hearts of indicated mice ( $n = 5$  per group). (H) Representative fluorescence images of left ventricle tissues stained with  $\alpha\text{SMA}$  and Collagen type 1 $\alpha$  antibodies as indicators of fibroblast activation and fibrosis. The scale bar is 100  $\mu\text{m}$ . \* $P < 0.05$ , \*\* $P < 0.01$  versus Sham operation groups, # $P < 0.05$ , ## $P < 0.01$  versus WT group after same operation. The data are shown as means  $\pm$  SEM. IVSTd, interventricular septal thickness at end-diastole; LVDD, left ventricular diameter at end-diastole; PWTd, posterior wall thickness at end-diastole; TAC, transverse aortic constriction.



accumulation was decreased in the TAC-operated heart of Cavin-2-KO mice compared with that of the WT mice (Figure 1H and Figure S1D).

### Cavin-2 promotes the trans-differentiation from fibroblast to myofibroblast

The roles of Cavin-2, including the caveolae morphology, in the fibroblasts, are still unknown. To explore the caveolae in the cardiac fibroblasts, we isolated primary cardiac fibroblasts to assess the relationship between Cavin-2 and the number of caveolae. The number of caveolae was significantly reduced in Cavin-2 KO cardiac fibroblasts compared with WT cardiac fibroblasts (Figure 2A). Single-cell RNA-seq data from the Tabula Muris Consortium<sup>27</sup> showed that Cavin-2 expression level in myofibroblasts is high in mouse heart tissues (Figure S2A). Therefore, we focused on the fibroblasts for the cardiac fibrosis associated with Cavin-2. We isolated MEFs from Cavin-2 KO and WT mice and evaluated trans-differentiation into myofibroblast, migration, and proliferation (Figure 2B and Figure S2B). Cavin-2 KO MEFs significantly attenuated TGF- $\beta$ 1-induced  $\alpha$ SMA expression compared with WT MEFs, suggesting the reduced trans-differentiation into myofibroblasts (Figure 2C, Figure S2C, and Figure S2D). TGF- $\beta$ 1-induced mRNA expression of fibrosis-associated genes was also significantly decreased in the Cavin-2 KO MEFs (Figure 2D). Migration, but not proliferation, was reduced in the Cavin-2 KO MEFs (Figure 2E and Figure S2E). On the contrary, Cavin-2 overexpression facilitated the trans-differentiation into myofibroblast and the mRNA expression of fibrosis-associated genes (Figure 2F–H).

### Cavin-2 deficiency in fibroblasts attenuates TGF- $\beta$ /Smad signalling

TGF- $\beta$  signalling activates fibrosis-associated gene expressions in fibroblasts via mobilization of transcription factors, Smad2/3. Therefore, we evaluated TGF- $\beta$ /Smad signalling and the transcription of plasminogen activator inhibitor-1 (PAI-1), one of its downstream genes. The PAI-1 is an ECM protease inhibitor and contributes to tissue ECM stabilization. Smad2/3 transfer into the nucleus by TGF- $\beta$ 1 was reduced in the Cavin-2 KO MEFs compared with that in the WT MEFs (Figure 3A). TGF- $\beta$ -induced Smad2 phosphorylation was significantly reduced in the Cavin-2 KO MEFs (Figure 3B). In contrast, the phosphorylation of Akt or ERK was no difference between the WT MEFs and the Cavin-2 KO MEFs (Figure S3). TGF- $\beta$ -induced *Pai-1* mRNA expression in the Cavin-2 KO MEFs was significantly decreased compared with the WT MEFs (Figure 3C). Similarly, the *Pai-1* mRNA expression after the TAC operation was considerably reduced in the Cavin-2 KO hearts compared with the WT hearts (Figure 3D). Using

proximity-dependent biotin identification, we screened for proteins that interact with Cavin-2 to explore the factors affecting with TGF- $\beta$ /Smad signalling. Biotin identification identified the proteins interacting with Cavin-2 in MEFs. The Volcano plot showed that HSP90 proteins interacted with Cavin-2 strongly (Figure 3E). A previous study has demonstrated that HSP90 regulates TGF- $\beta$  signalling by its ability to chaperone TGF- $\beta$  receptors.<sup>29</sup> The protein expression of HSP90 in the Cavin-2 KO MEFs was significantly decreased compared with that in the WT MEFs (Figure 3F). Our results suggested that Cavin-2 deficiency attenuates TGF- $\beta$ /Smad signalling by reducing HSP90 protein levels.

### Fibroblast-specific Cavin-2 cKO attenuates cardiac fibrosis resulting in the suppression of heart failure

To elucidate the role of Cavin-2 in fibroblasts in cardiac fibrosis, we generated activated fibroblast-specific Cavin-2 conditional KO (Cavin-2 cKO) mice and induced pressure-overload HF. The cardiac function was comparable in the Cavin-2 cKO mice and the Cavin-2<sup>flox/flox</sup> mice (Figure S4A). The peak pressure gradient at the transverse aorta was similar between Cavin-2<sup>flox/flox</sup> mice and Cavin-2 cKO mice operated with TAC (Figure S4B). The *postn* mRNA expression was significantly increased in the TAC-operated Cavin-2<sup>flox/flox</sup> mice than in the sham-operated Cavin-2<sup>flox/flox</sup> mice (Figure S4C). Systolic and diastolic functions of the heart 2 and 4 weeks after the TAC operation were preserved in the Cavin-2 cKO mice compared with the Cavin-2<sup>flox/flox</sup> mice (Figure 4B and Figure S4D). TAC-induced cardiac hypertrophy was reduced in the Cavin-2 cKO mice compared with the Cavin-2<sup>flox/flox</sup> mice (Figure 4C). Fibrotic area in the heart 4 weeks after the TAC operation was also significantly reduced in the Cavin-2 cKO mice (Figure 4D, Figure S4E). Furthermore, the degree of heart weight-to-body weight ratio (HW/BW) was positively correlated with the severity of fibrosis in the TAC-operated hearts. Cardiac fibrosis was consistently less from the early phase of cardiac hypertrophy in the Cavin-2 cKO mice compared with the Cavin-2<sup>flox/flox</sup> mice (Figure 4D). These results indicate that Cavin-2 in fibroblasts is preferentially involved in cardiac fibrosis than cardiac hypertrophy. The mRNA expression levels of cardiac remodelling and fibrosis-related genes were significantly suppressed in the Cavin-2 cKO mice compared with the Cavin-2<sup>flox/flox</sup> mice (Figure 4E).

## Discussion

In this study, we report that Cavin-2 in fibroblasts plays an essential role in the fibrotic remodelling of HF. Although the relationship between several caveolae-related proteins

**Figure 2** Cavin-2 promotes trans-differentiation from fibroblast to myofibroblast. (A) Representative electron micrographs of cardiac fibroblasts from WT and Cavin-2 KO mice and quantification of caveolae density ( $n = 7$  per group). The scale bar is 200 nm. (B) Schematic of the experimental design for mouse embryonic fibroblast (MEF) culture. (C) Representative fluorescence images of MEFs stained with phalloidin-FITC and  $\alpha$ SMA-Cy3, as indicators of myofibroblast and percentage of  $\alpha$ SMA positive cell ( $n = 3$  per group). The scale bar is 100  $\mu$ m. (D) Relative mRNA expression of genes associated with myofibroblast (*Acta2*) and fibrosis (*Ctgf*, *Col1a1*, and *Col3*) in MEFs ( $n = 3$  or 6 per group). (E) *In vitro* MEF migration quantification by scratch assay ( $n = 7$  per group). (F) Schematic of the experimental design for Cavin-2 overexpression in MEFs. (G) Representative fluorescence images of MEFs stained with phalloidin-FITC and  $\alpha$ SMA-Cy3. The scale bar is 100  $\mu$ m. (H) Relative mRNA expression of *Acta2* and *Ctgf* in MEFs ( $n = 6$  per group). \* $P < 0.05$ , \*\* $P < 0.01$  versus PBS groups, ## $P < 0.01$  versus WT group with same stimulation. The data are shown as mean  $\pm$  SEM.

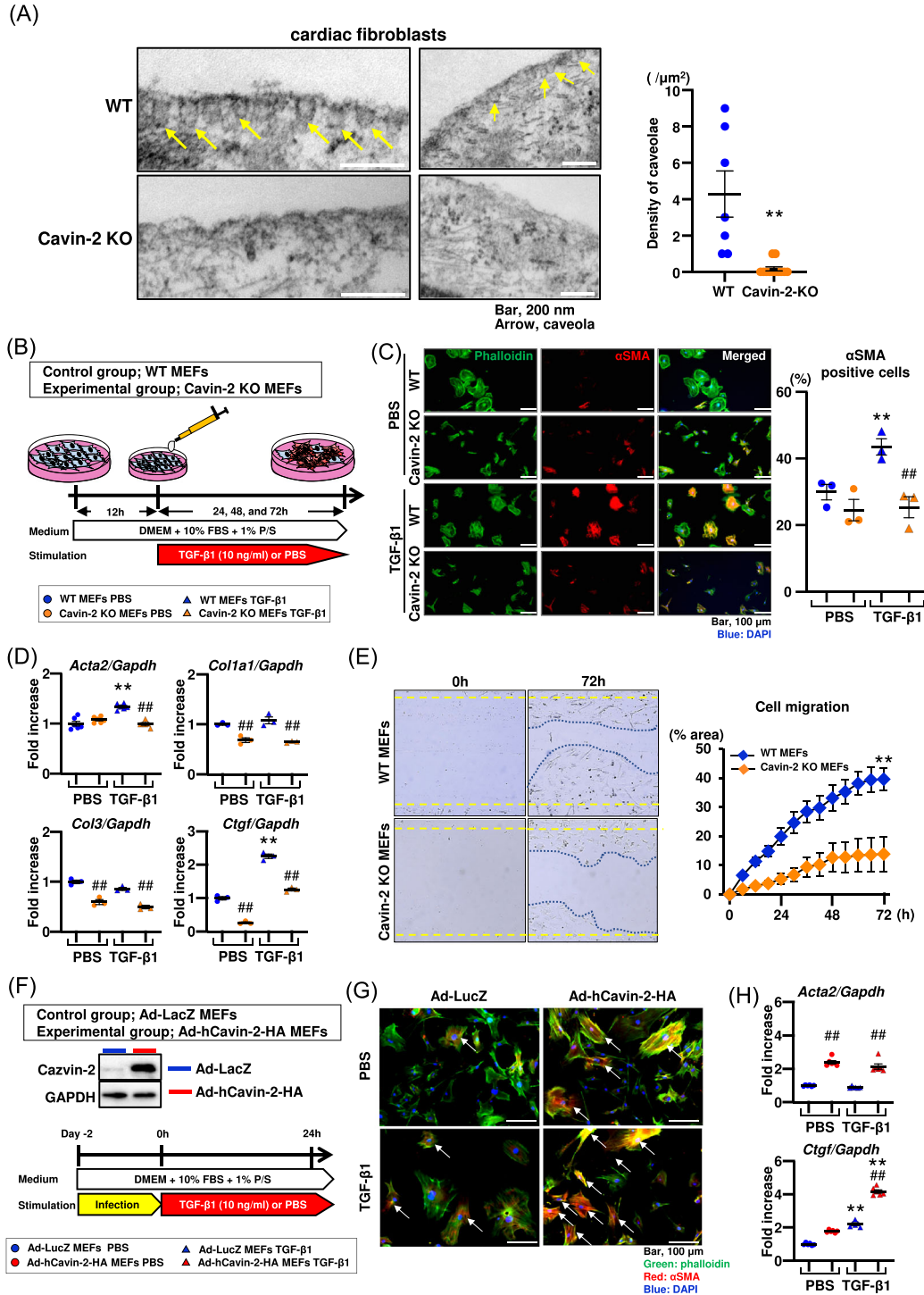


**Figure 3** Cavin-2 loss attenuates TGF- $\beta$ 1-induced Smad signalling in fibroblasts. (A) Representative fluorescence images of MEFs stained with  $\alpha$ SMA-Cy3 and pSmad2/3 antibodies. The bar is 100  $\mu$ m. (B) Representative western blot images (upper) and quantitation graph (lower) of Smad2 phosphorylation in MEFs ( $n = 3$  per group). Relative mRNA expression level of *Pai-1* as a downstream target of TGF- $\beta$ 1/Smad signalling in MEFs (C,  $n = 6$  per group) and mice after Sham or TAC operation (D,  $n = 5$  per group). (E) The Volcano plot about interacted proteins with Cavin-2 by the screening with BioID in MEFs. Each dot represents one protein. The orange dots are caveolae-related proteins (Cav-1, Cavin-1, and Cavin-2) that have already been reported to interact with Cavin-2. The red dots represent HSP90 proteins. (F) Representative western blot images (upper) and quantitation graph (lower) of HSP90 in MEFs ( $n = 4$  or 5 per group). \* $P < 0.05$ , \*\* $P < 0.01$  versus PBS groups, ### $P < 0.01$  versus WT group with same stimulation. The data are shown as mean  $\pm$  SEM.

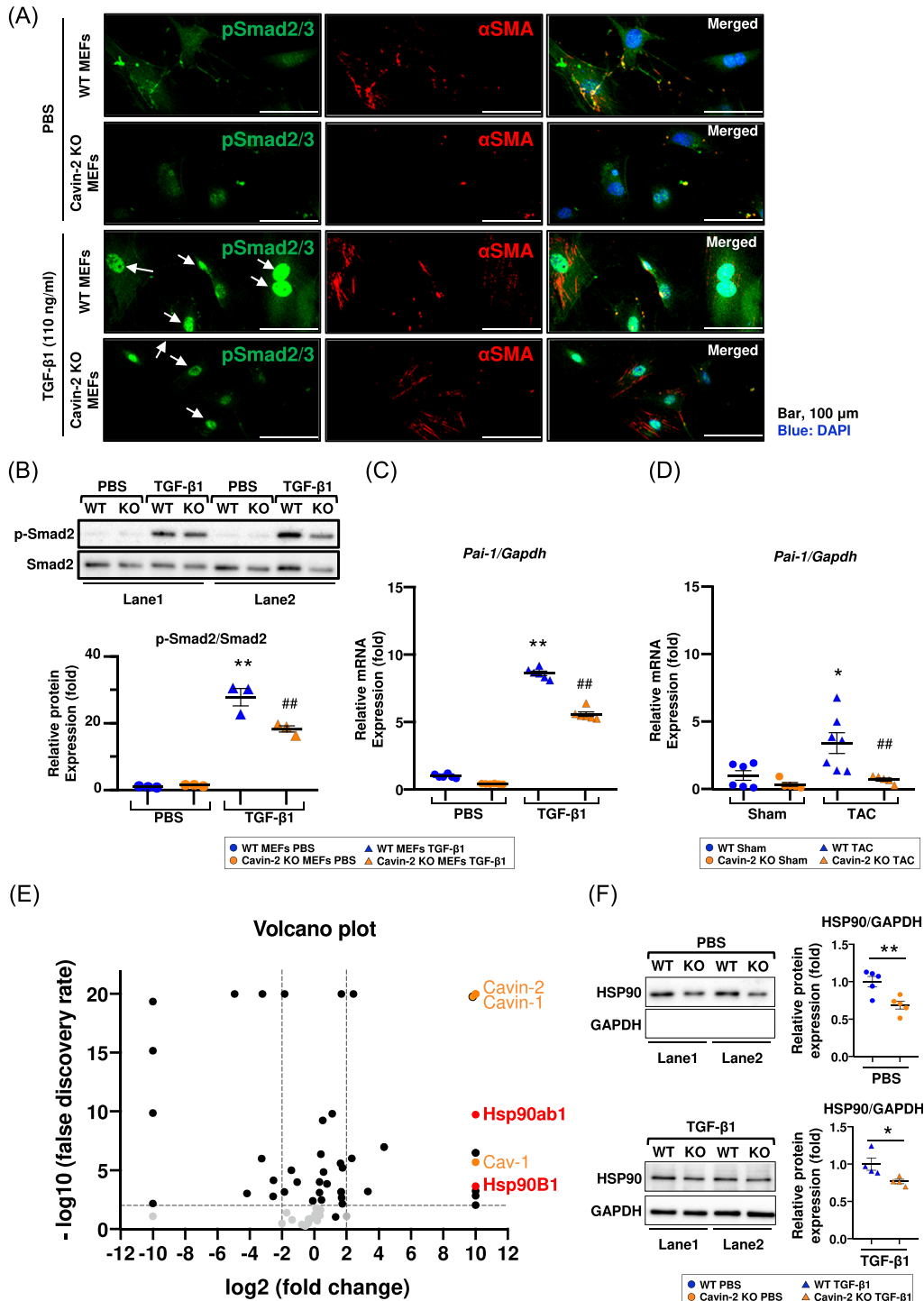
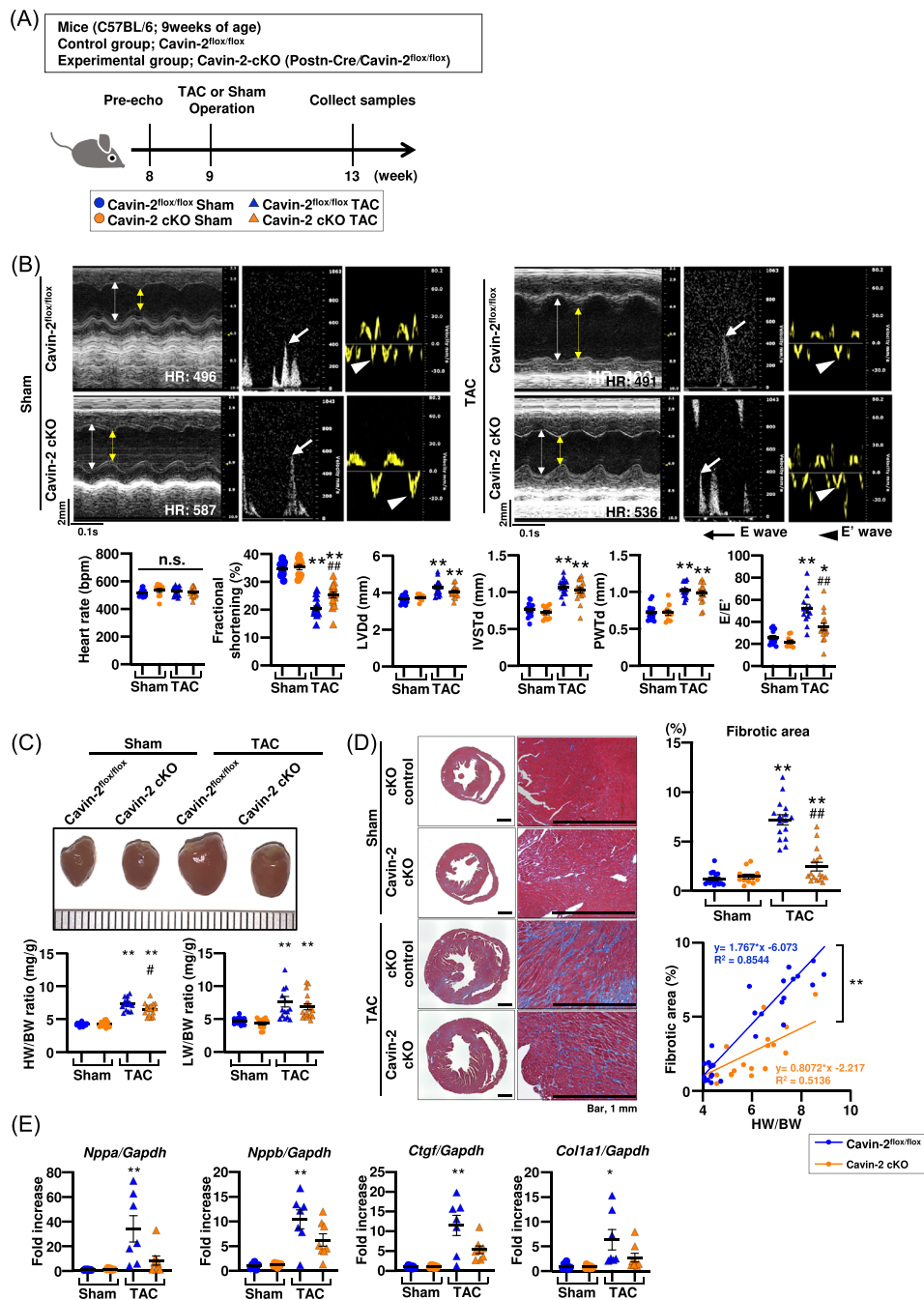




**Figure 4** Activated fibroblast-specific Cavin-2 cKO attenuates cardiac fibrosis and preserves left ventricular diastolic function. (A) Schematic of the experimental design for activated fibroblast-specific Cavin-2 cKO mice. (B) Representative M-mode images and data of echocardiography in Cavin-2<sup>fllox/fllox</sup> and Cavin-2 cKO mice 4 weeks after Sham and TAC operation. (C) Gross appearance of whole heart (upper row), and heart or lung weight/body weight ratio (mg/g) (lower graphs) in the mice (Cavin-2<sup>fllox/fllox</sup> Sham, *n* = 15; Cavin-2 cKO Sham, *n* = 12; Cavin-2<sup>fllox/fllox</sup> TAC, *n* = 15; Cavin-2 cKO TAC, *n* = 17). (D) Representative images of Masson's trichrome staining after 4 weeks of Sham or TAC operation, quantification of fibrotic area, and correlation diagram (Cavin-2<sup>fllox/fllox</sup> Sham, *n* = 15; Cavin-2 cKO Sham, *n* = 11; Cavin-2<sup>fllox/fllox</sup> TAC, *n* = 16; Cavin-2 cKO TAC, *n* = 16). The scale bar is 1 mm. (E) Relative expression of genes associated with heart failure (*Nppa*, *Nppb*) and fibrosis (*Ctgf* and *Col1a1*) in hearts of indicated mice (Cavin-2<sup>fllox/fllox</sup> Sham, *n* = 7; Cavin-2 cKO Sham, *n* = 8; Cavin-2<sup>fllox/fllox</sup> TAC, *n* = 7; Cavin-2 cKO TAC, *n* = 8). \**P* < 0.05, \*\**P* < 0.01 versus Sham operation groups, #*P* < 0.05, ##*P* < 0.01 versus Cavin-2<sup>fllox/fllox</sup> group after same operation. The data are shown as mean ± SEM. BW, body weight; E/E', the ratio of early diastolic mitral inflow velocity to early diastolic mitral annular velocity; HW, heart weight; IVSTd, interventricular septal thickness at end-diastole; LVdD, left ventricular diameter at end-diastole; LW, lung weight; PWTd, posterior wall thickness at end-diastole; TAC, transverse aortic constriction.



and HF has been previously reported, the role of Cavin-2 in HF remained unclear. Here, we demonstrate that fibroblast-specific deletion of Cavin-2 prevents adverse fibrotic remodelling and the progression of HF in a pressure-overloaded HF. Cavin-2 is expressed abundantly in fibroblasts in the heart and promotes fibroblast-to-myofibroblast trans-differentiation in HF. Cavin-2 deletion suppresses TGF- $\beta$ -induced Smad2/3 phosphorylation. HSP90, a regulator of TGF- $\beta$ /Smad signalling,<sup>29</sup> was decreased in Cavin-2 KO MEFs. Overall, Cavin-2 modulates TGF- $\beta$ /Smad signalling by reducing HSP90, promotes trans-differentiation from fibroblasts to myofibroblasts, and is involved in cardiac fibrosis.

There are various reports on the percentage of fibroblasts in the heart, but fibroblasts comprise a relatively large proportion of non-cardiomyocytes.<sup>30</sup> In addition, fibroblasts are important for myocardium injury and play pivotal roles in cardiac fibrosis, adverse remodelling, and arrhythmogenesis.<sup>31</sup> In the heart of patients with HF, myofibroblasts with  $\alpha$ -smooth muscle actin stress fibres are predominantly present in interstitial fibrosis.<sup>32</sup> Fibrosis is regulated by many complex pathways. Trans-differentiation into myofibroblasts is known to be regulated by changes in the mitochondrial biogenesis and transcriptional regulation of  $\alpha$ SMA via miRNAs.<sup>33,34</sup> In addition, it has been reported that cardiomyocyte-specific miRNAs translocate into fibroblasts in the form of exosomes, which cause myofibroblast activation.<sup>35</sup> In the present study, we demonstrated that Cavin-2 is associated with trans-differentiation of fibroblasts to myofibroblasts *in vitro*, and fibroblast-specific Cavin-2 deletion attenuated cardiac fibrosis *in vivo*. Although the mechanism details require further investigation, our results suggest that loss of Cavin-2 may suppress cardiac fibrosis by suppressing trans-differentiation from fibroblasts to myofibroblasts.

The TGF- $\beta$  signalling pathway regulates cardiac fibrosis, and various signalling are involved downstream of the TGF- $\beta$  pathway, including Smad2/3, ERK, p38, and Akt.<sup>36</sup> Muscleblind-like protein 1 (MBNL1) is increasingly recognized as a central regulator of fibrosis. Recently, MBNL1 was reported to regulate  $\alpha$ SMA by converging on SRF via its target p38.<sup>37</sup> As these signalling pathways are affected by TGF- $\beta$  receptor activation,<sup>38</sup> direct long-term inhibition of TGF- $\beta$  signalling can be a risk of unacceptable side effects in HF treatment.<sup>10</sup> On the other hand, selective blockade of Smad-dependent signalling in fibroblasts suppress the progression of cardiac fibrosis and HF.<sup>39</sup> HSP90 is one of the regulators of the TGF- $\beta$ /Smad signalling pathway. Inhibition of HSP90 suppresses the phosphorylation of Smad2/3, resulting in attenuation of the translocation of Smad2/3 into the nucleus and gene transcription.<sup>40</sup> In the present study, Cavin-2 deletion in MEFs reduced HSP90 protein expression levels and suppressed the phosphorylation of Smad2 and translocation of Smad2/3 into the nucleus. Deletion of Cavin-2 also attenuated the expression level of fibrosis-related genes and *Pai-1*, which is activated by Smad signal-

ling. Interestingly, Cavin-2 deletion only suppressed the phosphorylation of Smad2 but not that of ERK and Akt. Furthermore, systemic and fibroblast-specific Cavin-2 knockout did not impact cardiac function under normal conditions. Therefore, anti-fibrotic therapies targeting Cavin-2 may be a promising therapeutic approach to ameliorate HF without adversely affecting cardiac function.

Caveolae and caveolae-related proteins are associated with various cardiovascular diseases. Caveolin-1 and Cavolin-3, muscle-specific caveolin, are associated with HF via modulating intracellular signalling.<sup>41</sup> In addition, we have previously shown that Cavin-1 and Cavin-4, a muscle-specific caveolae component, affect the cardiac remodelling and fibrosis in cardiac hypertrophy and ischemia-reperfusion injury models.<sup>19,42,43</sup> In our previous report, we observed cardiomyocyte hypertrophy with increased phosphorylation of ERK in systemic Cavin-1 KO mice.<sup>19</sup> In the present study, up-regulation of ERK phosphorylation was not observed in systemic Cavin-2 KO mice. The absence of increased phosphorylation of ERK in the hearts of Cavin-2 KO mice might be one of the reasons that Cavin-2 KO mice do not reveal cardiac hypertrophy. Cavin-2 is highly expressed in the adipose tissue, lung, and heart<sup>44</sup> and is involved in caveolae number and morphology in endothelial cells. In the present study, we confirmed that the deletion of Cavin-2 decreased the caveolae even in cardiac fibroblasts. Cavin-2 has been reported to affect various intracellular signalling and receptor stability in endothelial cells.<sup>22</sup> We also reported that Cavin-2 in adipocytes stabilizes insulin receptors and enhances Akt signalling in promoting adipogenesis and lipid metabolism.<sup>23</sup> In addition to these reports, the present study demonstrated that Cavin-2-regulated cell migration and trans-differentiation into myofibroblasts via TGF- $\beta$ /Smad signalling and fibroblast-specific Cavin-2 deletion reduced cardiac fibrosis in pressure-overloaded HF and maintains cardiac function. Our findings provide a previously undescribed function of Cavin-2 in cardiac fibrosis and novel insights into the underlying pathogenetic mechanisms of HF.

In this study, we focused on trans-differentiation of fibroblasts. Although it would be ideal to assess trans-differentiation using cardiac fibroblasts, primarily adult cardiac fibroblasts express  $\alpha$ SMA rapidly without TGF- $\beta$  treatment *in vitro* and are unsuitable for determining trans-differentiation. On the other hand, MEFs, isolated from 13–14 days pregnant mice, maintain low  $\alpha$ SMA expression levels and well response to TGF- $\beta$  treatment. Thus, we performed trans-differentiation analysis using MEFs in this study. A limitation of this study is that it was impossible to evaluate trans-differentiation using cardiac fibroblasts *in vitro*. The precise role of Cavin-2 in the mechanisms of cardiac fibrosis remains elucidated. Further studies are needed to clarify the role of Cavin-2 in cardiac fibrosis.

In summary, we first demonstrated that fibroblast-specific deletion of Cavin-2 prevents adverse fibrotic remodelling in

the TAC model. Cavin-2 may be involved in trans-differentiation from fibroblast into myofibroblast through TGF- $\beta$ /Smad signalling. Our results suggest that Cavin-2 in fibroblasts is a potential therapeutic target for cardiac fibrosis.

## Conflict of interest

The authors declare that there is no conflict of interest.

## Funding

This work was supported in part by the Japan Society for the Promotion of Science Grants-in-Aid for Scientific Research (JSPS KAKENHI) (JP18K07046) and National Institutes of Health (R01 HL159436).

## References

- Travers JG, Kamal FA, Robbins J, Yutzey KE, Blaxall BC. Cardiac fibrosis: The fibroblast awakens. *Circ Res* 2016;**118**:1021-1040. doi:10.1161/CIRCRESAHA.115.306565
- Virani SS, Alonso A, Benjamin EJ, Bittencourt MS, Callaway CW, Carson AP, et al. Heart disease and stroke statistics-2020 update: A report from the American Heart Association. *Circulation* 2020;**141**:e139-e596. doi:10.1161/CIR.0000000000000757
- Meagher PB, Lee XA, Lee J, Visram A, Friedberg MK, Connelly KA. Cardiac fibrosis: Key role of integrins in cardiac homeostasis and remodeling. *Cell* 2021;**10**:770. doi:10.3390/cells10040770
- Sweeney M, Corden B, Cook SA. Targeting cardiac fibrosis in heart failure with preserved ejection fraction: Mirage or miracle? *EMBO Mol Med* 2020;**12**:e10865. doi:10.15252/emmm.2019.10865
- Zannad F, Rossignol P, Iraqi W. Extracellular matrix fibrotic markers in heart failure. *Heart Fail Rev* 2010;**15**:319-329. doi:10.1007/s10741-009-9143-0
- Zannad F, Alla F, Dousset B, Perez A, Pitt B. Limitation of excessive extracellular matrix turnover may contribute to survival benefit of spironolactone therapy in patients with congestive heart failure: Insights from the randomized aldactone evaluation study (RALES). Rales investigators. *Circulation* 2000;**102**:2700-2706. doi:10.1161/01.cir.102.22.2700
- Spinale FG. Myocardial matrix remodeling and the matrix metalloproteinases: Influence on cardiac form and function. *Physiol Rev* 2007;**87**:1285-1342. doi:10.1152/physrev.00012.2007
- Moore-Morris T, Guimarães-Camboa N, Banerjee I, Zambon AC, Kisseleva T, Velayoudon A, et al. Resident fibroblast lineages mediate pressure overload-induced cardiac fibrosis. *J Clin Invest* 2014;**124**:2921-2934. doi:10.1172/JCI74783
- Khan R, Sheppard R. Fibrosis in heart disease: Understanding the role of transforming growth factor-beta in cardiomyopathy, valvular disease and arrhythmia. *Immunology* 2006;**118**:10-24. doi:10.1111/j.1365-2567.2006.02336.x
- Gyorfi AH, Matei AE, Distler JHW. Targeting TGF-beta signaling for the treatment of fibrosis. *Matrix Biol* 2018;**68-69**:8-27. doi:10.1016/j.matbio.2017.12.016
- Noh H, J Kim H, R Yu M, Kim WY, Kim J, Ryu J, et al. Heat shock protein 90 inhibitor attenuates renal fibrosis through degradation of transforming growth factor-beta type II receptor. *Lab Invest* 2012;**92**:1583-1596. doi:10.1038/labinvest.2012.127
- Tomcik M, Zerr P, Pitkowski J, Palumbo-Zerr K, Avouac J, Distler O, et al. Heat shock protein 90 (Hsp90) inhibition targets canonical TGF-beta signalling to prevent fibrosis. *Ann Rheum Dis* 2014;**73**:1215-1222. doi:10.1136/annrheumdis-2012-203095
- Zhang K, Lu Y, Yang P, Li C, Sun H, Tao D, et al. HILI inhibits TGF-beta signaling by interacting with Hsp90 and promoting Tbetar degradation. *PLoS ONE* 2012;**7**:e41973. doi:10.1371/journal.pone.0041973
- Sibinska Z, Tian X, Korfei M, Kojonazarov B, Kolb JS, Klepetko W, et al. Amplified canonical transforming growth factor-beta signalling via heat shock protein 90 in pulmonary fibrosis. *Eur Respir J* 2017;**49**:1501941. doi:10.1183/13993003.01941-2015
- Sontake V, Wang Y, Kasam RK, Sinner D, Reddy GB, Naren AP, et al. Hsp90 regulation of fibroblast activation in pulmonary fibrosis. *JCI Insight* 2017;**2**:e91454. doi:10.1172/jci.insight.91454
- Razani B, Zhang XL, Bitzer M, von Gersdorff G, Böttinger EP, Lisanti MP. Caveolin-1 regulates transforming growth factor (TGF)-beta/SMAD signaling through an interaction with the TGF-beta type I receptor. *J Biol Chem* 2001;**276**:6727-6738. doi:10.1074/jbc.M008340200
- Strippoli R, Loureiro J, Moreno V, Benedicto I, Pérez Lozano ML, Barreiro O, et al. Caveolin-1 deficiency induces a MEK-ERK1/2-Snail-1-dependent epithelial-mesenchymal transition and fibrosis during peritoneal dialysis. *EMBO Mol Med* 2015;**7**:102-123. doi:10.15252/emmm.201404127
- Huang X, Pan L, Pu H, Wang Y, Zhang X, Li C, et al. Loss of caveolin-1 promotes endothelial-mesenchymal transition during sepsis: A membrane proteomic study. *Int J Mol Med* 2013;**32**:585-592. doi:10.3892/ijmm.2013.1432
- Taniguchi T, Maruyama N, Ogata T, Kasahara T, Nakanishi N, Miyagawa K, et al. PTRF/Cavin-1 deficiency causes cardiac dysfunction accompanied by cardiomyocyte hypertrophy and cardiac

## Supporting information

Additional supporting information may be found online in the Supporting Information section at the end of the article.

**Figure S1.** The cardiac function with systemic Cavin-2 KO mice before TAC operation, and the change of mRNA expression and cardiac fibrosis after TAC operation.

**Figure S2.** Expression of Cavin-2 in each cell type and evaluation of  $\alpha$ SMA expression and mitotic potential in Cavin-2 KO MEF.

**Figure S3.** Phosphorylation of noncanonical TGF- $\beta$  signalling in Cavin-2 KO MEFs.

**Figure S4.** The cardiac function in Cavin-2 cKO mice before and 2 weeks after TAC operation.

**Figure S5.** The uncropped membranes with MWmarkers.

**Table S1.** The list of primer sequences used for RT-qPCR.

- fibrosis. *PLoS ONE* 2016;**11**:e0162513. doi:10.1371/journal.pone.0162513
20. Ogata T, Ueyama T, Isodono K, Tagawa M, Takehara N, Kawashima T, *et al.* MURC, a muscle-restricted coiled-coil protein that modulates the rho/ROCK pathway, induces cardiac dysfunction and conduction disturbance. *Mol Cell Biol* 2008;**28**:3424-3436. doi:10.1128/MCB.02186-07
  21. Gustincich S, Vatta P, Goruppi S, Wolf M, Saccone S, Della Valle G, *et al.* The human serum deprivation response gene (SDPR) maps to 2q32-q33 and codes for a phosphatidylserine-binding protein. *Genomics* 1999;**57**:120-129. doi:10.1006/geno.1998.5733
  22. Boopathy GTK, Kulkarni M, Ho SY, Boey A, Chua EWM, Barathi VA, *et al.* Cavin-2 regulates the activity and stability of endothelial nitric-oxide synthase (eNOS) in angiogenesis. *J Biol Chem* 2017;**292**:17760-17776. doi:10.1074/jbc.M117.794743
  23. Higuchi Y, Ogata T, Nakanishi N, Nishi M, Sakamoto A, Tsuji Y, *et al.* Requirement of Cavin-2 for the expression and stability of IRbeta in adequate adipocyte differentiation. *Mol Metab* 2022;**55**:101416. doi:10.1016/j.molmet.2021.101416
  24. Lindsley A, Snider P, Zhou H, Rogers R, Wang J, Olaopa M, *et al.* Identification and characterization of a novel Schwann and outflow tract endocardial cushion lineage-restricted periostin enhancer. *Dev Biol* 2007;**307**:340-355. doi:10.1016/j.ydbio.2007.04.041
  25. Okawa Y, Hoshino A, Ariyoshi M, Kaimoto S, Tateishi S, Ono K, *et al.* Ablation of cardiac TIGAR preserves myocardial energetics and cardiac function in the pressure overload heart failure model. *Am J Physiol Heart Circ Physiol* 2019;**316**:H1366-H1377. doi:10.1152/ajpheart.00395.2018
  26. Durkin ME, Qian X, Popescu NC, Lowy DR. Isolation of mouse embryo fibroblasts. *Bio Protoc* 2013;**3**:3. doi:10.21769/bioproto.908
  27. The Tabula Muris Consortium, Overall coordination, Logistical coordination, Organ collection and processing, Library preparation and sequencing, Computational data analysis, *et al.* Single-cell transcriptomics of 20 mouse organs creates a Tabula Muris. *Nature* 2018;**562**:367-372. doi:10.1038/s41586-018-0590-4
  28. Mechold U, Gilbert C, Ogrzyzko V. Codon optimization of the BirA enzyme gene leads to higher expression and an improved efficiency of biotinylation of target proteins in mammalian cells. *J Biotechnol* 2005;**116**:245-249. doi:10.1016/j.jbiotec.2004.12.003
  29. Wrighton KH, Lin X, Feng XH. Critical regulation of TGFbeta signaling by Hsp90. *Proc Natl Acad Sci U S A* 2008;**105**:9244-9249. doi:10.1073/pnas.0800163105
  30. Bergmann O, Zdunek S, Felker A, Salehpour M, Alkass K, Bernard S, *et al.* Dynamics of cell generation and turnover in the human heart. *Cell* 2015;**161**:1566-1575. doi:10.1016/j.cell.2015.05.026
  31. Zhou P, Pu WT. Recounting cardiac cellular composition. *Circ Res* 2016;**118**:368-370. doi:10.1161/CIRCRESAHA.116.308139
  32. Nagaraju CK, Robinson EL, Abdeselem M, Trenson S, Dries E, Gilbert G, *et al.* Myofibroblast phenotype and reversibility of fibrosis in patients with end-stage heart failure. *J Am Coll Cardiol* 2019;**73**:2267-2282. doi:10.1016/j.jacc.2019.02.049
  33. Emelyanova L, Sra A, Schmuck EG, Raval AN, Downey FX, Jahangir A, *et al.* Impact of statins on cellular respiration and de-differentiation of myofibroblasts in human failing hearts. *ESC Heart Fail* 2019;**6**:1027-1040. doi:10.1002/ehf2.12509
  34. Wang X, Morelli MB, Matarese A, Sardu C, Santulli G. Cardiomyocyte-derived exosomal microRNA-92a mediates post-ischemic myofibroblast activation both in vitro and ex vivo. *ESC Heart Fail* 2020;**7**:284-288. doi:10.1002/ehf2.12584
  35. Morelli MB, Shu J, Sardu C, Matarese A, Santulli G. Cardiosomal microRNAs are essential in post-infarction myofibroblast phenoconversion. *Int J Mol Sci* 2019;**21**:201. doi:10.3390/ijms210201
  36. Maruyama K, Imanaka-Yoshida K. The pathogenesis of cardiac fibrosis: a review of recent progress. *Int J Mol Sci* 2022;**23**:2617. doi:10.3390/ijms23052617
  37. Nelson AR, Bugg D, Davis J, Saucerman JJ. Network model integrated with multi-omic data predicts MBNL1 signals that drive myofibroblast activation. *iScience* 2023;**26**:106502. doi:10.1016/j.isci.2023.106502
  38. Hall C, Gehmlich K, Denning C, Pavlovic D. Complex relationship between cardiac fibroblasts and cardiomyocytes in health and disease. *J Am Heart Assoc* 2021;**10**:e019338. doi:10.1161/JAHA.120.019338
  39. Khalil H, Kanisicak O, Prasad V, Correll RN, Fu X, Schips T, *et al.* Fibroblast-specific TGF-beta-Smad2/3 signaling underlies cardiac fibrosis. *J Clin Invest* 2017;**127**:3770-3783. doi:10.1172/JCI94753
  40. Lee J, An YS, Kim MR, Kim YA, Lee JK, Hwang CS, *et al.* Heat shock protein 90 regulates subcellular localization of Smads in Mv1Lu cells. *J Cell Biochem* 2016;**117**:230-238. doi:10.1002/jcb.25269
  41. Gratton JP, Bernatchez P, Sessa WC. Caveolae and caveolins in the cardiovascular system. *Circ Res* 2004;**94**:1408-1417. doi:10.1161/01.RES.0000129178.56294.17
  42. Ogata T, Naito D, Nakanishi N, Hayashi YK, Taniguchi T, Miyagawa K, *et al.* MURC/Cavin-4 facilitates recruitment of ERK to caveolae and concentric cardiac hypertrophy induced by alpha1-adrenergic receptors. *Proc Natl Acad Sci U S A* 2014;**111**:3811-3816. doi:10.1073/pnas.1315359111
  43. Nishi M, Ogata T, Cannistraci CV, Ciucci S, Nakanishi N, Higuchi Y, *et al.* Systems network genomic analysis reveals cardioprotective effect of MURC/Cavin-4 deletion against ischemia/reperfusion injury. *J Am Heart Assoc* 2019;**8**:e012047. doi:10.1161/JAHA.119.012047
  44. Hansen CG, Shvets E, Howard G, Riento K, Nichols BJ. Deletion of cavin genes reveals tissue-specific mechanisms for morphogenesis of endothelial caveolae. *Nat Commun* 2013;**4**:1831. doi:10.1038/ncomms2808